Original Article

A prediction model based on dual-layer spectral detector computed tomography for distinguishing nonluminal from luminal invasive breast cancer

Jun Liu[#], Lanlan Wang[#], Zhaodong Ai, Lian Jian, Ming Yang, Siye Liu, Xiaoping Yu

Department of Radiology, The Affiliated Cancer Hospital of Xiangya School of Medicine, Central South University/Hunan Cancer Hospital, Changsha, China

Contributions: (I) Conception and design: J Liu, S Liu, X Yu; (II) Administrative support: X Yu; (III) Provision of study materials or patients: J Liu, L Wang, S Liu; (IV) Collection and assembly of data: L Wang, L Jian, M Yang; (V) Data analysis and interpretation: J Liu, Z Ai; (VI) Manuscript writing: All authors; (VII) Final approval of manuscript: All authors.

[#]These authors contributed equally to this work.

Correspondence to: Xiaoping Yu, MD; Siye Liu, PhD. Department of Radiology, The Affiliated Cancer Hospital of Xiangya School of Medicine, Central South University/Hunan Cancer Hospital, 283 Tongzipo Road, Yuelu District, Changsha 410006, China. Email: yuxiaoping@hnca.org.cn; 136069792@qq.com.

Background: The identification of the molecular subtypes of breast cancer is critical to determining appropriate treatment strategies and assessing prognosis. This study aimed to evaluate the ability of dual-layer spectral detector computed tomography (DLCT) metrics to differentiate luminal from nonluminal invasive breast cancer.

Methods: A total of 220 patients with invasive breast cancer who underwent routine DLCT examination were included in the study. The molecular subtypes of breast cancer were identified through immunohistochemical staining of biopsies or postoperative pathological specimens. DLCT quantitative parameters were compared between the luminal and nonluminal types of breast cancer. The diagnostic efficacy of these parameters was determined via receiver operating characteristic (ROC) curves. Univariate and multivariate regression analyses were conducted to identify independent predictors that could differentiate nonluminal from luminal breast cancer. A nomogram prediction model was established based on multivariate regression analysis. The performance of the nomogram model was assessed with ROC curve and calibration curve analyses.

Results: Among the DLCT quantitative values, eight were significantly lower in the luminal type than in the nonluminal type of breast cancer (P<0.001–0.011). The area under the curve (AUC) values for these significant DLCT quantitative parameters ranged from 0.604 to 0.694. Multivariate logistic regression analysis identified CT-reported lymph node metastasis status [hazard ratio (HR) =4.214; P<0.001], the Hounsfield unit (HU) value of the virtual monoenergetic image at 40 keV (HU_{VMI40}) (HR =2.628; P=0.012), and the normalized iodine concentration (nIC) (HR =2.182; P=0.041) as independent predictors of the nonluminal type, with an AUC of 0.754 [95% confidence interval (CI): 0.688–0.820]. The nomogram based on multivariate logistic regression analysis exhibited good discrimination and calibration (Hosmer-Lemeshow test; P=0.835). An average AUC value of 0.75 was obtained for the internal validation data.

Conclusions: DLCT quantitative parameters are valuable noninvasive indexes for differentiating between the luminal and nonluminal types of invasive breast cancer. Furthermore, the nomogram constructed in this study could guide individualized predictions of molecular subtypes in patients with invasive breast cancer.

Keywords: Dual-layer spectral detector computed tomography (DLCT); breast cancer; molecular subtype; nonluminal type; nomogram

Submitted Mar 24, 2024. Accepted for publication Sep 18, 2024. Published online Nov 11, 2024.
doi: 10.21037/qims-24-598
View this article at: https://dx.doi.org/10.21037/qims-24-598

Introduction

Breast cancer is a prevalent malignant disease among women and has surpassed lung cancer as the leading cause of cancer-related deaths among females. It has caused 685,000 deaths annually, and approximately 2.3 million new cases were reported worldwide in 2020 (1). Moreover, currently, clinical predictive indicators, such as histological and tumor-node-metastasis (TNM) staging, have been widely applied for risk evaluation in patients with invasive breast cancer. However, due to substantial heterogeneity, even patients with the same TNM and histological stages can exhibit significant variations in clinical manifestations, treatment responses, and prognosis (2). At present, with advancements in sequencing technology and immunohistochemistry techniques, the detection of molecular subtypes in invasive breast cancer has provided valuable information for predicting treatment response and the risk of recurrence and metastasis.

Based on the expression level of receptors, breast cancer can be divided into the luminal A, luminal B, human epidermal growth factor receptor 2 (HER2)-enriched, and triple-negative (TN) molecular subtypes (3). Furthermore, each subtype is distinct in terms of its clinical features and prognosis. Luminal breast cancer, which includes the luminal A and B subtypes, is the most common type, is less malignant, and has a lower risk of recurrence than the other types. Additionally, this type, despite being less sensitive to chemotherapy, exhibits a positive response to endocrine and targeted therapies, ultimately leading to a favorable prognosis. In contrast, nonluminal breast cancer, including the HER2-enriched and TN subtypes, is more malignant and has a higher risk of recurrence, often resulting in lymph node metastasis. This type is initially sensitive to chemotherapy but is associated with a poor prognosis (4,5). Therefore, accurately distinguishing the molecular subtype of invasive breast cancer before treatment can aid in formulating appropriate clinical treatment plans and in assessing prognosis.

Currently, the primary approach for identifying the molecular subtype of breast cancer involves immunohistochemical staining to detect the expression of estrogen receptor (ER), progesterone receptor (PR), HER2, and Ki-67 (6). However, this approach requires either an invasive pretreatment biopsy or postoperative pathological examination. Moreover, the biology of breast cancer can change over time and in response to treatment, leading to alterations in receptor status and molecular subtype (7). Therefore, the development of a noninvasive method that can predict the molecular subtype of breast cancer as a supplement to pathological examination would be invaluable in guiding the optimal treatment for this cancer.

The emergence of dual-layer spectral detector computed tomography (DLCT), which is based on double-layer spectral detector technology, has enabled the reconstruction of conventional images and spectral maps through a single scan, such as virtual monoenergetic images (VMI), iodine concentration (IC) images, and effective atomic number (Z_{eff}) maps. This can be useful for the qualitative analysis of lesions via the comparison of various parameters such as computed tomography (CT) and standard deviation (SD) values, as well as the slope of the spectral Hounsfield unit (HU) attenuation curve (λ_{HU}) at different energy levels of lesions. Due to these technological advancements, CT has been applied in multiparameter joint diagnosis. This approach has shown promise in improving the detection rate of lesions and can provide a reference for distinguishing between benign and malignant tumors. Furthermore, it assists in the formulation of treatment plans and the evaluation of antitumor efficacy (8-12). However, there is a limited amount of research on the application of DLCT in breast cancer. A retrospective study with individual quantitative parameters demonstrated that the HU value of the VMI at 40 keV (HU_{VMI40}) on delayed-phase imaging can improve the visibility of breast cancer lesions, potentially aiding in breast cancer diagnosis (13). Additionally, a recent study demonstrated that quantitative parameters derived from DLCT correlate with the levels of hormone receptor expression in breast cancer (14). However, to our knowledge, no studies have examined the ability of DLCT

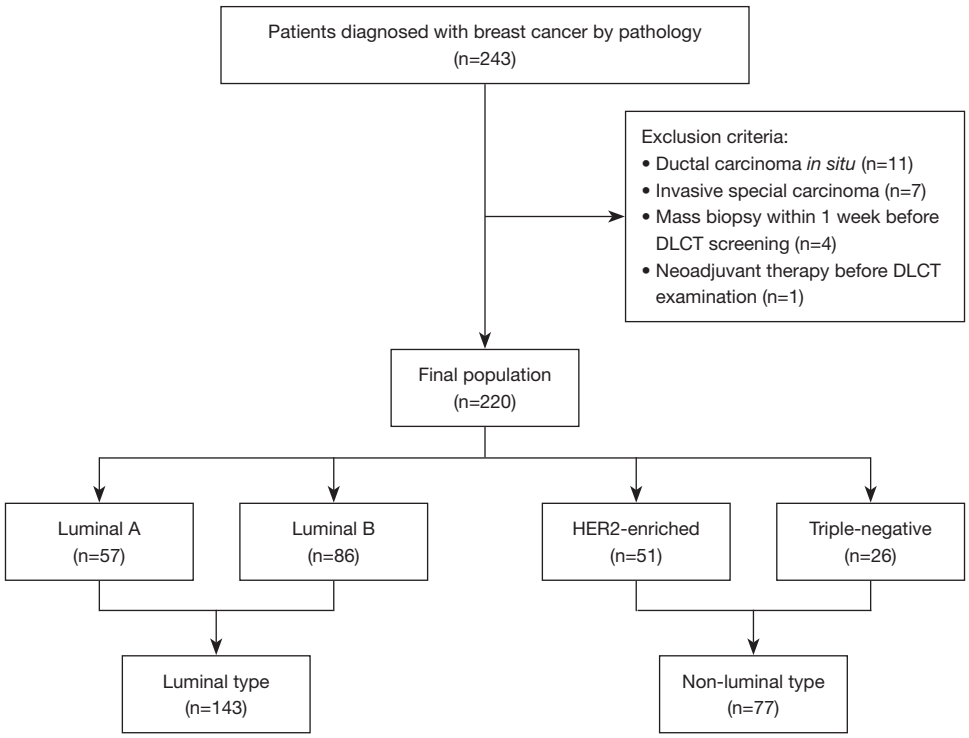

Figure 1 Flowchart of the patient selection. DLCT, dual-layer spectral detector computed tomography; HER2, human epidermal growth factor receptor 2.

to differentiate between luminal and nonluminal breast cancer. Therefore, this study aimed to evaluate whether quantitative parameters derived from DLCT could serve as predictive biomarkers for distinguishing between the luminal and nonluminal types of invasive breast cancer. Furthermore, a prediction model based on DLCT was developed to distinguish between the nonluminal and luminal types. We present this article in accordance with the TRIPOD reporting checklist (available at https://qims.amegroups.com/article/view/10.21037/qims-24-598/rc).

Methods

Patients

This single-center, retrospective study was approved by the Medical Ethics Committee of Hunan Cancer Hospital (No. 202260) and was conducted in accordance with the Declaration of Helsinki (as revised in 2013). Written informed consent was waived due to the retrospective nature of the analysis. Patients diagnosed with invasive breast cancer who received contrast-enhanced chest CT with DLCT between July 2022 and April 2023 were included. The primary purpose of contrast-enhanced CT was to evaluate potential pulmonary, mediastinal, and axillary lymph node metastases. The primary inclusion criteria for patients were as follows: (I) diagnosed with invasive breast cancer through needle biopsy or surgical pathology and (II) completion of DLCT examination for invasive breast cancer at the Affiliated Cancer Hospital of Xiangya School of Medicine, Central South University/Hunan Cancer Hospital. Meanwhile, the exclusion criteria were as follows: (I) diagnosed with ductal carcinoma *in situ* based on histopathology, (II) presence of specific invasive carcinoma subtypes such as mucinous carcinoma or medullary carcinoma, (III) completion of mass biopsy within 1 week before the DLCT examination, and (IV) previous antitumor treatment for breast cancer before DLCT examination. In total, 220 patients from our hospital were included in this study. The flowchart of patient selection is presented in *Figure 1*.

DLCT image acquisition

CT imaging data were acquired using a DLCT scanner

(IQon Spectral CT, Philips Healthcare, Amsterdam, the Netherlands). Patients were scanned craniocaudally in the supine position, and the scanning range was from the lung tip to the lung base. The scanning parameters were as follows: tube voltage, 120 kVp; automated current modulation; pitch, 0.609; collimation, 64×0.625 mm; rotation time, 0.5 seconds; and nonenhanced scans performed first. Subsequently, the iodinated nonionic contrast media (iohexol; Omnipaque 350, GE HealthCare, Chicago, IL, USA) was administered via peripheral vein at a dosage of 1.5 mL/kg with a flow rate of 2 mL/s, which was followed by a 30-mL saline injected at the same rate. No serious adverse reactions occurred after the injection of Omnipaque in any of the patients. Moreover, the bolus-tracking technique was used to control individual contrast injection timing. After the threshold of 100 HU set in the aortic arch was reached, the venous-phase scan began with an additional delay of 60 seconds. After scanning, the conventional CT and spectral base images were simultaneously generated, with a slice thickness of 1 mm and slice increment of 1 mm.

Processing and analysis of the DLCT quantitative parameters

The acquired venous-phase data of breast cancer were retrospectively analyzed using a spectral workstation (IntelliSpace Portal version 9.0, Philips Healthcare). A radiologist (Z.A., with more than 10 years of experience in breast and chest diagnostic imaging) who was blinded to the histopathologic results of the breast cancers placed a circular region of interest as large as possible in the homogeneous density area of the mass on its maximum dimension image, avoiding areas of necrosis, calcification, and blood vessels. The quantitative parameters, including HU value of virtual monoenergetic images at 40 keV (HU_{VMI40}) and 70 keV (HU_{VMI70}), IC, Z_{eff}, HU value of virtual noncontrast (VNC) images, and electron density (ED) were measured. In addition, these quantitative parameters of invasive breast cancer were divided by the corresponding parameters of HU_{VMI40}, IC, Z_{eff}, VNC, and ED of the aorta at the same slice of the breast mass. This allowed for the retrieval of normalized HU_{VMI40} (nHU_{VMI40}), IC (nIC), Z_{eff} (nZ_{eff}), VNC (nVNC), and ED (nED). Moreover, the λ_{HU} (15) and $HU_{\Delta VMI40}$ were calculated as follows:

$$\lambda_{HU} = \left(HU_{VMI40} - HU_{VMI70}\right)/30 \quad [1]$$

$$HU_{\Delta VMI40} = HU_{VMI40} - HU_{VNC} \quad [2]$$

Representative cases are shown in *Figure 2*.

Clinical and histopathological analysis

All patients enrolled received a biopsy or postoperative pathological examination of their breast mass. Breast cancer specimens were stained with hematoxylin and eosin (HE). Immunohistochemical staining results, including ER, PR, HER2, and Ki-67, were evaluated to further distinguish the molecular subtypes. The status of ER and PR was evaluated as positive when >1% of the nuclei were positively stained (16,17). The HER2 status was as determined as follows: an immunohistochemical staining intensity score ≥0 or 1+ indicated a negative status, while a score of 3+ indicated a positive status. An immunohistochemical HER2 score of 2+ was further evaluated by fluorescence *in situ* hybridization, and if *HER2* gene amplification was observed, the molecular status was considered HER2 positive (18). The Ki-67 status was classified as positive if staining occurred in ≥20% of cells and as negative if staining occurred in <20% (19). Based on the expression level of ER, PR, HER2, and Ki-67, breast cancers were classified as the luminal A (ER and/or PR+, HER2−, and Ki-67−), luminal B (ER and/or PR+, HER2−, and Ki-67+; or ER and/or PR+, HER2+, and Ki-67 at any level), HER2-enriched (ER−, PR−, and HER2+), or TN subtype (ER−, PR−, and HER2−) (17). The luminal type includes luminal A and B subtypes, while the nonluminal type includes HER2-enriched and TN subtypes. Molecular subtypes and histopathology results were reviewed independently by one pathologist (Xiaoyan Chen) with more than 10 years of experience.

Clinical data, such as age, T stage, CT-reported tumor size, CT-reported lymph node metastasis status, and distant metastasis stage were recorded. Moreover, the criteria for a CT diagnosis of lymph node metastasis were as follows: a lymph node with round shape or an irregular shape with a fuzzy edge, a short-axis diameter over 5 mm, a long axis:short axis ratio of less than 2:1, and obvious enhancement on enhancement scanning or disappearance of the lymphatic structure (20,21).

Statistical analysis

Statistical analysis was performed using R software version 3.5.1 (The R Foundation for Statistical Computing, Vienna,

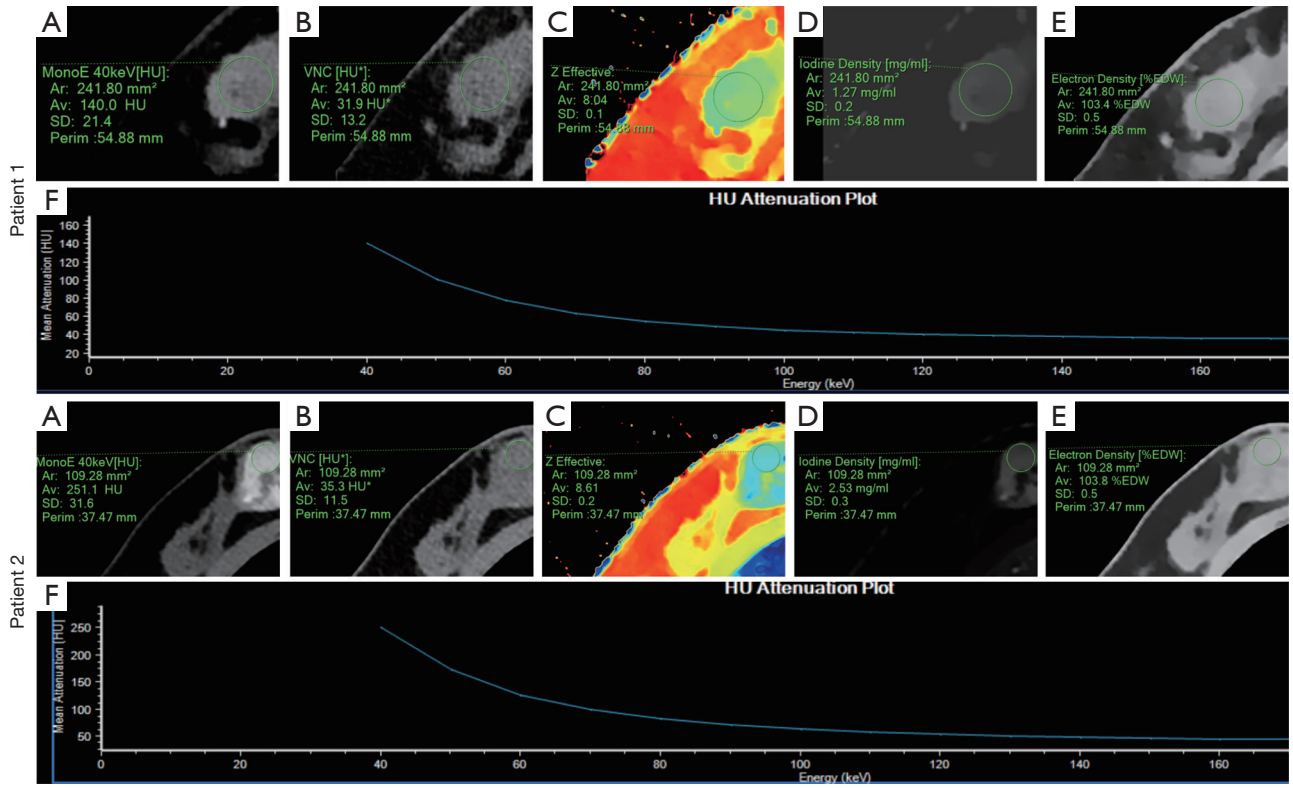

Figure 2 The DLCT images of representative cases. Patient 1: representative DLCT images from a 51-year-old woman with the luminal A subtype of right invasive ductal carcinoma. Patient 2: representative DLCT images from a 46-year-old woman with the HER2-enriched subtype of right invasive ductal carcinoma. (A) VMI40. (B) VNC. (C) Z_{eff}. (D) IC. (E) ED map. (F) The spectral HU attenuation curve. MonoE, monoenergetic; HU, Hounsfield unit; Ar, area; Av, average; SD, standard deviation; DLCT, dual-layer spectral detector computed tomography; HER2, human epidermal growth factor receptor 2; VMI40, virtual monoenergetic image at 40 keV; VNC, virtual noncontrast image; Z_{eff}, effective atomic number image; IC, iodine concentration image; ED, electron density.

Austria) and SPSS 20 (IBM Corp., Armonk, NY, USA). The normality of continuous variables was tested using the Kolmogorov-Smirnov test. Continuous variables of clinical and DLCT parameters with a normal distribution were analyzed with the independent samples *t*-tests and were presented as the mean ± SD. Variables with a nonnormal distribution were analyzed with the Mann-Whitney test and were presented as the median and interquartile range (IQR). Receiver operating characteristic (ROC) curve analysis was used to evaluate the differential diagnostic efficacy of DLCT parameters for the luminal and nonluminal types, and the optimal threshold was determined according to the Youden index. To screen the significant DLCT parameters for the discrimination of these two types, univariate and multivariate regression analyses were conducted, and hazard ratios (HRs) were calculated. Based on the multivariate regression analysis, a nomogram prediction model was established. The predictive efficacy of the nomogram model was evaluated using an ROC curve. The calibration curve was assessed with Hosmer-Lemeshow goodness-of-fit test to evaluate the nomogram calibration. Furthermore, the nomogram model was internally validated using the 10-fold cross-validation method. A two-tailed P value <0.05 was considered statistically significant.

Results

Clinical and pathological characteristics

A total of 220 patients with pathologically proven invasive breast cancers were enrolled in this study (mean age 51 years; range, 28–77 years). Among these invasive breast cancers, 143 (65%) were categorized as the luminal type (luminal A + luminal B), and 77 (35%) were categorized

Table 1 Baseline characteristics of the 220 patients with invasive breast cancer

Characteristic	Value
Age (years), mean ± SD	51.88±10.14
CT-reported maximum tumor diameter (mm), mean ± SD	28.75±14.51
T stage, n (%)	
T1	55 (25)
T2	137 (62.3)
T3	14 (6.4)
T4	14 (6.4)
CT-reported lymph node metastasis status, n (%)	
Positive	134 (60.9)
Negative	86 (39.1)
M stage, n (%)	
M1	11 (5)
M0	209 (95)
Clinical TNM stage, n (%)	
I	27 (12.3)
II	108 (49.1)
III	74 (33.6)
IV	11 (5)
Histologic type, n (%)	
Invasive ductal carcinoma	216 (98.1)
Invasive lobular carcinoma	4 (1.9)
ER, n (%)	
Positive	143 (65)
Negative	77 (35)
PR, n (%)	
Positive	129 (58.6)
Negative	91 (41.4)
HER2, n (%)	
Positive	97 (44.1)
Negative	123 (55.9)
Ki-67 (%), mean ± SD	37.75±20.11
Molecular type, n (%)	
Luminal A	57 (25.9)
Luminal B	86 (39.1)
HER2-enriched	51 (23.2)
Triple-negative	26 (11.8)

SD, standard deviation; CT, computed tomography; TNM, tumor-node-metastasis; ER, estrogen receptor; PR, progesterone receptor; HER2, human epidermal growth factor receptor 2.

as the nonluminal type (HER2-enriched + TN) based on immunohistochemical staining results. The pathological and detailed clinical characteristics are shown in *Table 1*.

Differentiation between the luminal and nonluminal subtypes of breast cancer

The DLCT quantitative parameters and comparison of results between the luminal and nonluminal types are shown in *Table 2*. The HU_{VMI40}, nHU_{VMI40}, $HU_{\Delta VMI40}$, λ_{HU}, IC, nIC, Z_{eff}, and nZ_{eff} values of the luminal type were significantly lower than those of the nonluminal type (P<0.001–0.011). No significant differences were observed in the VNC, nVNC, ED, or nED values between the luminal and nonluminal types (P=0.262–0.637).

By conducting ROC curve analysis, the area under the curve (AUC) of these significant DLCT quantitative parameters (HU_{VMI40}, nHU_{VMI40}, $HU_{\Delta VMI40}$, λ_{HU}, IC, nIC, Z_{eff} and nZ_{eff}) for distinguishing between the nonluminal and luminal types ranged from 0.604 to 0.694. Additionally, among the parameters mentioned above, the highest differential diagnostic capability was observed in IC, with an AUC of 0.694, a sensitivity of 74.0%, and a specificity of 57.3% (*Table 3*, *Figure 3*).

Based on the cutoff values of these significant DLCT parameters, these invasive breast cancers were classified into low- and high-score groups. Univariate logistic regression analysis indicated that the following eight parameters were significantly associated with nonluminal type: HU_{VMI40} (P<0.001), nHU_{VMI40} (P<0.001), $HU_{\Delta VMI40}$ (P<0.001), λ_{HU} (P<0.001), IC (P<0.001), nIC (P<0.001), Z_{eff} (P<0.001), and nZ_{eff} (P=0.006). Regarding clinical characteristics, only the CT-reported lymph node metastasis status was found to be a predictor for differentiating between the nonluminal and luminal types of invasive breast cancer [HR =4.076, 95% confidence interval (CI): 2.123–7.826; P<0.001].

Development and evaluation of the nomogram prediction model

Multivariate logistic regression analysis indicated that the independent predictors of the nonluminal subtype were CT-reported lymph node metastasis status (HR =4.214; 95% CI: 2.120–8.377; P<0.001), HU_{VMI40} (HR =2.628; 95% CI: 1.239–5.574; P=0.012), and nIC (HR =2.182, 95% CI: 0.883–5.392; P=0.041) (*Table 4*). The nomogram prediction model based on these results for nonluminal subtypes (*Figure 4A*) yielded an AUC of 0.754 (95% CI: 0.688–0.820)

Table 2 Comparison of DLCT quantitative parameters between the luminal and non-luminal types of breast cancer

Parameter	Luminal type	Non-luminal type	*t*/*Z* value	P value
HU_{VMI40} (HU)	147.3 (116.4, 179.9)	176.2 (144.6, 227.1)	−4.681[z]	<0.001
HU_{nVMI40} (HU)	0.168 (0.132, 0.256)	0.230 (0.160, 0.363)	−3.659[z]	<0.001
$HU_{\Delta VMI40}$ (HU)	110.1 (75.7, 139.5)	137.50 (105.15, 187.55)	−4.729[z]	<0.001
λ_{HU} (HU/keV)	2.00±0.07	2.55±0.10	−4.43[t]	<0.001
VNC (HU*)	38.71±0.51	39.12±0.71	−0.473[t]	0.637
nVNC	0.905 (0.798, 1.021)	0.925 (0.788, 1.101)	−0.702[z]	0.483
IC (mg/mL)	1.28 (0.87, 1.67)	1.61 (1.315, 2.220)	−4.732[z]	<0.001
nIC	0.132 (0.095, 0.208)	0.184 (0.125, 0.305)	−4.023[z]	<0.001
Z_{eff}	8.024±0.023	8.237±0.032	−5.24[t]	<0.001
nZ_{eff}	0.732 (0.708, 0.786)	0.762 (0.719, 0.843)	−2.536[z]	0.011
ED (%EDW)	104.0 (103.7, 104.4)	104.1 (103.8, 104.5)	−0.985[z]	0.324
nED	0.984±0.0008	0.986±0.001	−1.125[t]	0.262

[z], Mann-Whitney U-test, with values expressed as the median (interquartile range); [t], the Welch *t*-test, with values expressed as the mean ± standard deviation. DLCT, dual-layer spectral detector computed tomography; HU_{VMI40}, HU value of virtual monoenergetic image at 40 keV; HU_{nVMI40}, normalized parameter of virtual monoenergetic image at 40 keV; $HU_{\Delta VMI40}$, = HU_{VMI40} − HU_{VNC}; λ_{HU}, slope of the spectral Hounsfield unit attenuation curve; VNC, virtual noncontrast; nVNC, normalized parameter of virtual noncontrast; IC, iodine concentration; nIC, normalized parameter of iodine concentration; Z_{eff}, effective atomic number; nZ_{eff}, normalized parameter of effective atomic number; ED, electron density; nED, normalized parameter of electron density.

Table 3 Diagnostic performance of DLCT quantitative parameters for the luminal and non-luminal types of breast cancer

Parameter	AUC (95%CI)	Cutoff value	Sensitivity	Specificity
HU_{VMI40} (HU)	0.691 (0.626–0.752)	159.9	0.675	0.643
HU_{nVMI40} (HU)	0.650 (0.583–0.713)	0.148	0.831	0.419
$HU_{\Delta VMI40}$ (HU)	0.693 (0.628–0.754)	117.5	0.714	0.608
λ_{HU} (HU/keV)	0.663 (0.596–0.725)	1.962	0.740	0.531
IC (mg/mL)	0.694 (0.628–0.754)	1.33	0.740	0.573
nIC	0.665 (0.598–0.727)	0.115	0.857	0.412
Z_{eff}	0.690 (0.624–0.750)	8.09	0.688	0.601
nZ_{eff}	0.604 (0.536–0.669)	0.759	0.519	0.671

DLCT, dual-layer spectral detector computed tomography; AUC, area under the curve; CI, confidence interval; HU_{VMI40}, HU value of virtual monoenergetic image at 40 keV; HU_{nVMI40}, normalized parameter of virtual monoenergetic image at 40 keV; $HU_{\Delta VMI40}$, = HU_{VMI40} − HU_{VNC}; λ_{HU}, slope of the spectral HU curve; IC, iodine concentration; nIC, normalized parameter of iodine concentration; Z_{eff}, effective atomic number; nZ_{eff}, normalized parameter of effective atomic number.

(*Figure 4B*). The nomogram score was calculated as follows:

$$\text{Nomogram score} = -2.654 \times (\text{intercept}) + 0.966 \times \text{VMI}_{40} + 0.780 \times \text{nIC} + 1.438 \times \text{N stage} \quad [3]$$

The calibration curve of the nomogram's ability to predict the nonluminal type had a high degree of consistency between the actual observation and predicted results (*Figure 4C*). The Hosmer-Lemeshow test showed no significant statistical difference between the calibration curve and ideal curve (P=0.835), indicating good model fit. Internal validation showed that the average AUC was 0.75

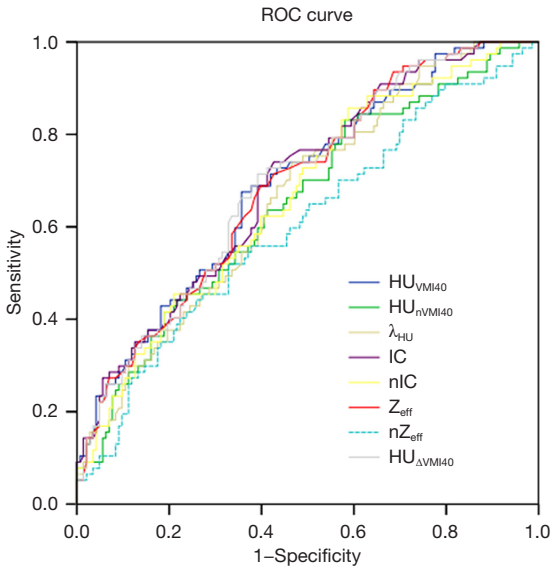

Figure 3 ROC curves of the DLCT quantitative parameters, including HU_{VMI40}, HU_{nVMI40}, λ_{HU}, IC, nIC, Z_{eff}, nZ_{eff}, and $HU_{\Delta VMI40}$, in differentiating between luminal and non-luminal types of breast cancer. ROC, receiver operating characteristic; HU_{VMI40}, HU value of virtual monoenergetic image at 40 keV; HU_{nVMI40}, normalized parameter of virtual monoenergetic image at 40 keV; λ_{HU}, slope of the spectral Hounsfield unit attenuation curve; IC, iodine concentration; nIC, normalized parameter of iodine concentration; Z_{eff}, effective atomic number; nZ_{eff}, normalized parameter of effective atomic number; $HU_{\Delta VMI40}$, = HU_{VMI40} – HU_{VNC}; DLCT, dual-layer spectral detector computed tomography.

(range, 0.70–0.86) according to the 10-fold cross-validation method.

Discussion

In this study, our objective was to evaluate the potential value of DLCT quantitative parameters in differentiating between the luminal and nonluminal types of invasive breast cancer. There were significant differences in certain DLCT parameters between these two types of breast cancer. We further developed a nomogram based on multivariate logistic regression analysis, which proved to be an efficient tool for accurately differentiating the nonluminal from luminal types of invasive breast cancer. Additionally, internal validation demonstrated that the model had good performance.

In recent years, there has been a growing body of research focusing on noninvasive methods for predicting the molecular subtype of breast cancer at early stages. Various imaging modalities, such as ultrasound, mammography, magnetic resonance imaging (MRI), and metabolic imaging, have been investigated for their correlation with molecular subtypes (22-27). Horvat *et al.* (23) demonstrated that the maximum apparent diffusion coefficient (ADC) in MRI serves as a quantitative imaging biomarker for the differentiation of luminal from nonluminal breast cancer. An *et al.* (24) reported that intratumor T2-weighted high signal intensity and rim enhancement on MRI were related to the TN subtype of breast cancer. Moreover, metabolic imaging can be used to monitor metabolic abnormalities in tumor cells. A study by Miyake *et al.* (26) found that the value of maximum standardized uptake value (SUV_{max}) in positron emission tomography-CT was an independent predictor for identifying the luminal A type of breast cancer. In contrast to these imaging methods and their disadvantages, contrast-enhanced DLCT may be a substantially efficient and noninvasive alternative for predicting the molecular subtype of breast cancer. In our study, the values of HU_{VMI40}, nHU_{VMI40}, $HU_{\Delta VMI40}$, λ_{HU}, IC, nIC, Z_{eff}, and nZ_{eff} were found to be higher in the nonluminal type than in the luminal type of breast cancer (all P values <0.05). Regarding HU_{VMI40}, a recent study demonstrated that breast cancer, as compared to benign nodules, on VMI40 yielded a higher conspicuity and mean HU value. Moreover, the mean HU_{VMI40} was significantly higher in breast cancer with a higher malignant degree (13), which is consistent with our finding that high HU_{VMI40} was an independent predictor of nonluminal type. Furthermore, IC represents the actual iodine content in enhanced DLCT images, which can reflect the blood supply and enhancement characteristics of tissues more accurately than can CT values and help provide information about the distribution of blood vessels in tumors (10,28). The corrected result of IC is nIC, which can further reduce individual differences among patients, thereby reflecting the distribution of blood vessels in the lesion more accurately. We observed that both IC and nIC were higher in the nonluminal type of breast cancer compared to the luminal type. This finding may be attributed to the fact that higher-grade breast cancers exhibit more aggressive growth, leading to increased tumor microvascular density and neovascularization. Consequently, the permeability of tumor vessels to contrast agents, such as iodine, is enhanced, resulting in greater iodine absorption in the lesion area (29-31).

In our study, the nonluminal type could be distinguished

Table 4 Univariate and multivariate logistic regression analyses for the differentiation of the non-luminal from the luminal subtype of breast cancer

Variables	Univariate analysis		Multivariate analysis	
	P	HR (95% CI)	P	HR (95% CI)
Age (years)	0.761	1.004 (0.977–1.032)		
CT-reported maximum tumor diameter	0.230	1.012 (0.993–1.031)		
T stage (T1/T2/T3/T4)	0.111	1.347 (0.934–1.942)		
CT-reported lymph node metastasis status (positive/negative)	<0.001	4.076 (2.123–7.826)	<0.001	4.214 (2.120–8.377)
M stage (M1/M0)	0.459	1.586 (0.468–5.374)		
Clinical stage (I/II/III/IV)	0.140	1.325 (0.912–1.925)		
HU_{VMI40} (low *vs.* high)	<0.001	3.752 (2.086–6.749)	0.012	2.628 (1.239–5.574)
HU_{nVMI40} (low *vs.* high)	<0.001	3.559 (1.798–7.042)		
$HU_{\Delta VMI40}$ (low *vs.* high)	<0.001	3.884 (2.137–7.061)		
λ_{HU} (low *vs.* high)	<0.001	3.233 (1.763–5.927)		
IC (low *vs.* high)	<0.001	3.831 (2.086–7.035)		
nIC (low *vs.* high)	<0.001	4.214 (2.052–8.657)	0.041	2.182 (0.883–5.392)
Z_{eff} (low *vs.* high)	<0.001	3.332 (1.852–5.993)		
nZ_{eff} (low *vs.* high)	0.006	2.208 (1.252–3.893)		

HR, hazard ratio; CI, confidence interval; CT, computed tomography; HU_{VMI40}, HU value of virtual monoenergetic image at 40 keV; HU_{nVMI40}, normalized parameter of virtual monoenergetic image at 40 keV; $HU_{\Delta VMI40}$, = HU_{VMI40} – HU_{VNC}; λ_{HU}, slope of the spectral HU curve; IC, iodine concentration; nIC, normalized parameter of iodine concentration; Z_{eff}, effective atomic number; nZ_{eff}, normalized parameter of effective atomic number.

from the luminal type via Z_{eff}, nZ_{eff}, and λ_{HU}. Generally, Z_{eff} is a measure of the compound atom within a material or mixture although its exact clinical significance has not yet been clarified (29). In their study, Wang *et al.* (30) found that the HER2-positive group had higher nZ_{eff} values in the venous phase compared to the HER2-negative group, and nZ_{eff} was positively correlated with Ki-67, a marker of proliferation. Meanwhile, λ_{HU} is generated via the correspondence of CT values to different keV levels, which can reflect the relationship between the mass absorption coefficient of tissues and different X-ray energy levels (32). Quantitative information concerning tissue composition can be provided by λ_{HU}, which was reported in one study to be higher in malignant lesions than in benign lesions of the breast, with the best differential diagnostic capability in the venous phase (29). In our study, the λ_{HU} value of the nonluminal type was higher, which is likely because the composition of nonluminal type is more malignant than is the luminal type; moreover, the blood supply of the former is more abundant, which can also absorb more iodine after the injection of the iodine contrasting agent.

Clinical characteristics, including CT-reported tumor diameter, age, T stage, CT-reported lymph node metastasis status, metastasis staging, and clinical stage, were evaluated in this study. Among them, the CT-reported lymph node metastasis status was the only predictor significantly related to the nonluminal type of invasive breast cancer. Our findings are similar to those of previous studies reporting that the nonluminal type of breast cancer, with higher malignancy, is associated with a greater risk of lymph node metastasis (4,5). At present, the morphological features of lymph nodes in CT images, such as short axis, aspect ratio, shape, degree of enhancement, and the structure of lymphatics, are often used to evaluate the status of axillary lymph nodes in patients with breast cancer. Furthermore, the CT-reported lymph node metastasis status can be

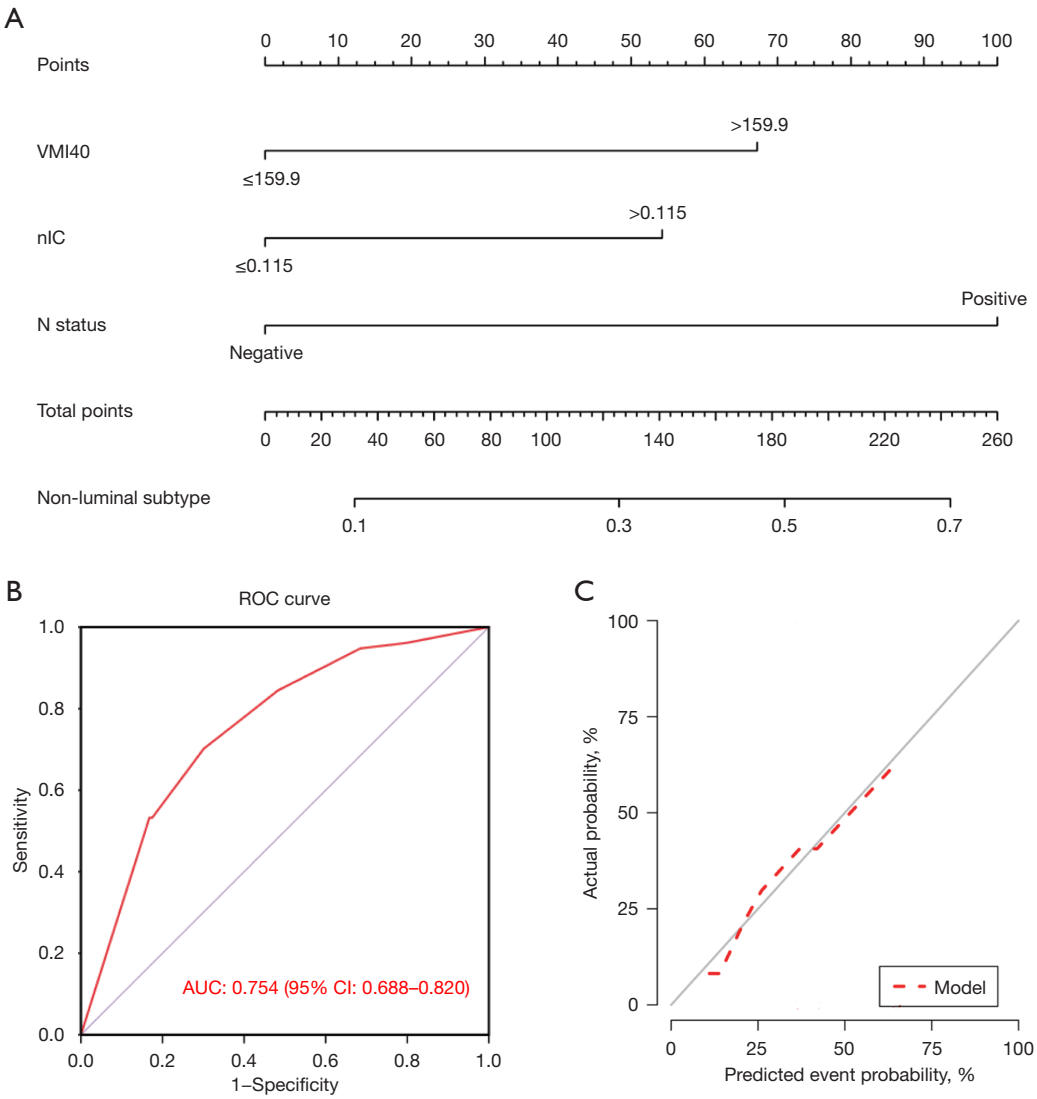

Figure 4 Nomogram model establishment and predictive performance evaluation. (A) The nomogram model based on DLCT quantitative parameters for predicting the non-luminal type. An upward vertical line is first drawn according to the value of VMI40, nIC, and N status to determine the corresponding score. The total points are calculated as the sum of the three scores described above. Finally, based on the sum, a downward vertical line is drawn from the "Total Points" line to "Non-luminal subtype" to determine the probability of the non-luminal type. (B) ROC curve for predicting the non-luminal type. (C) Calibration curve of the nomogram model. The X-axis represents the predicted probability, and the Y-axis is the actual probability for the non-luminal type. VMI40, virtual monoenergetic image at 40 keV; nIC, normalized parameter of iodine concentration; ROC, receiver operating characteristic; AUC, area under the curve; CI, confidence interval; DLCT, dual-layer spectral detector computed tomography.

conveniently obtained before treatment.

In our study, we found that two DLCT parameters, HU_{VMI40} and nIC, were independent predictors of the nonluminal type of invasive breast cancer. This suggests that these two parameters are more relevant for differentiating between the luminal and nonluminal types. By incorporating these parameters with the CT-reported lymph node metastasis status, we developed a comprehensive nomogram to predict the molecular subtypes of invasive breast cancer, which yielded an AUC

of 0.754. In a previous study, the ADC in MRI was used as an imaging biomarker for the differentiation of luminal and nonluminal types of breast cancer, yielding an AUC of 0.685 (23). However, our nomogram demonstrated a higher diagnostic efficacy (AUC =0.754). Therefore, DLCT parameters may be more effective than ADC for predicting the molecular subtypes of breast cancer. Additionally, the calibration curve of the nomogram also verified that the predictive probability of the model fit well with the actual molecular subtypes of breast cancer, indicating that this model has high accuracy.

Chest CT examinations are essential in the screening, preoperative evaluation, and postoperative follow-up of breast tumors. They offer numerous advantages, including their simplicity, speed, noninvasiveness, and patient acceptance. The National Comprehensive Cancer Network (NCCN) guidelines recommend the routine use of contrast-enhanced CT of the chest as part of preoperative examinations for patients with breast cancer. The DLCT examination adopted in this study obtained conventional CT images and DLCT quantitative parameters without increasing the patients' radiation dose and financial burden. As an added benefit, the breast, mediastinum, and lung conditions could be observed simultaneously in a single examination, providing more useful imaging information for the diagnosis and treatment of breast tumors. Furthermore, in this study, patients were scanned in the supine position, which is the same as that used during breast cancer surgery and which contrasts the prone position typically used in MRI examinations. Additionally, being aligned with the surgical position, the DLCT examination minimized the potential image and lesion deviations caused by changes in body position.

Certain limitations to this study should be addressed. First, the proportions of luminal type breast cancer and invasive lobular carcinoma of the breast in this study were relatively low compared to those in other research (33). Additionally, as this was a single-center, retrospective study conducted over a specific time period with a limited number of patients (N=220), selection bias might have been present. Therefore, future prospective studies with larger, multicenter cohorts are necessary to validate the predictive performance of the model. Second, we did not include arterial phase CT scans, and thus a comparison between DLCT parameters in the venous and arterial phases is lacking. However, the purpose of the single-phase enhanced DLCT scanning in this study was to exclude intrapulmonary, mediastinal, and axillary lymphatic metastases. By focusing on the venous phase, we could minimize the radiation dose and financial burden for patients in accordance with ethical norms. Moreover, previous studies have shown that DLCT quantitative parameters at the venous stage are highly valuable for predicting the molecular subtypes of invasive breast cancer (14,29). Finally, the study lacked radiomics data of DLCT images. Recent studies have demonstrated the potential of radiomics as a noninvasive tool for distinguishing between the luminal and non-luminal types of breast cancer (34,35). However, this study focused on developing a nomogram prediction model based solely on clinical characteristics and DLCT parameters. This approach simplifies the application process and avoids potential statistical inefficiencies, making it more suitable for clinical implementation and promotion.

Conclusions

Our study identified significant differences in multiple DLCT parameters between the luminal and non-luminal types of breast cancer. Furthermore, the nomogram constructed in this study may be a useful, noninvasive tool for guiding the individualized prediction of the molecular subtypes of invasive breast cancer.

Acknowledgments

The authors thank Dr. Xiaoyan Chen (expert in pathology, The Affiliated Cancer Hospital of Xiangya School of Medicine, Central South University, China) for providing the pathological analysis, and Dr. Weiwei Deng (Clinical and Technical Support, Philips Healthcare China) for providing technical support of DLCT.

Funding: This work was supported by the Scientific Research Project of the Hunan Provincial Health Commission (No. 202109011033; Changsha, China), and Hunan Cancer Hospital Climb Plan (No. ZX2021004-3; Changsha, China).

Footnote

Reporting Checklist: The authors have completed the TRIPOD reporting checklist. Available at https://qims.amegroups.com/article/view/10.21037/qims-24-598/rc

Conflicts of Interest: All authors have completed the ICMJE

uniform disclosure form (available at https://qims.amegroups.com/article/view/10.21037/qims-24-598/coif). The authors have no conflicts of interest to declare.

Ethical Statement: The authors are accountable for all aspects of the work in ensuring that questions related to the accuracy or integrity of any part of the work are appropriately investigated and resolved. This study was conducted in accordance with the Declaration of Helsinki (as revised in 2013) and was approved by the Medical Ethics Committee of Hunan Cancer Hospital (No. 202260). Written informed consent was waived due to the retrospective nature of the analysis.

References

1. Sung H, Ferlay J, Siegel RL, Laversanne M, Soerjomataram I, Jemal A, Bray F. Global Cancer Statistics 2020: GLOBOCAN Estimates of Incidence and Mortality Worldwide for 36 Cancers in 185 Countries. CA Cancer J Clin 2021;71:209-49.
2. Martelotto LG, Ng CK, Piscuoglio S, Weigelt B, Reis-Filho JS. Breast cancer intra-tumor heterogeneity. Breast Cancer Res 2014;16:210.
3. Esposito A, Criscitiello C, Curigliano G. Highlights from the 14(th) St Gallen International Breast Cancer Conference 2015 in Vienna: Dealing with classification, prognostication, and prediction refinement to personalize the treatment of patients with early breast cancer. Ecancermedicalscience 2015;9:518.
4. Łukasiewicz S, Czeczelewski M, Forma A, Baj J, Sitarz R, Stanisławek A. Breast Cancer-Epidemiology, Risk Factors, Classification, Prognostic Markers, and Current Treatment Strategies-An Updated Review. Cancers (Basel) 2021;13:4287.
5. Lobbezoo DJ, van Kampen RJ, Voogd AC, Dercksen MW, van den Berkmortel F, Smilde TJ, van de Wouw AJ, Peters FP, van Riel JM, Peters NA, de Boer M, Borm GF, Tjan-Heijnen VC. Prognosis of metastatic breast cancer subtypes: the hormone receptor/HER2-positive subtype is associated with the most favorable outcome. Breast Cancer Res Treat 2013;141:507-14.
6. Szymiczek A, Lone A, Akbari MR. Molecular intrinsic versus clinical subtyping in breast cancer: A comprehensive review. Clin Genet 2021;99:613-37.
7. Pisco AO, Huang S. Non-genetic cancer cell plasticity and therapy-induced stemness in tumour relapse: 'What does not kill me strengthens me'. Br J Cancer 2015;112:1725-32.
8. Jamali S, Michoux N, Coche E, Dragean CA. Virtual unenhanced phase with spectral dual-energy CT: Is it an alternative to conventional true unenhanced phase for abdominal tissues? Diagn Interv Imaging 2019;100:503-11.
9. Chen ML, Shi AH, Li XT, Wei YY, Qi LP, Sun YS. Is there any correlation between spectral CT imaging parameters and PD-L1 expression of lung adenocarcinoma? Thorac Cancer 2020;11:362-8.
10. Lennartz S, Le Blanc M, Zopfs D, Große Hokamp N, Abdullayev N, Laukamp KR, Haneder S, Borggrefe J, Maintz D, Persigehl T. Dual-Energy CT-derived Iodine Maps: Use in Assessing Pleural Carcinomatosis. Radiology 2019;290:796-804.
11. Zeng F, Chen L, Lin L, Hu H, Li J, He P, Wang C, Xue Y. Iodine map histogram metrics in early-stage breast cancer: prediction of axillary lymph node metastasis status. Quant Imaging Med Surg 2022;12:5358-70.
12. Meyer S, Liu LP, Litt HI, Halliburton SS, Shapira N, Noël PB. Phantom-based quantification of the spectral accuracy in dual-layer spectral CT for pediatric imaging at 100 kVp. Quant Imaging Med Surg 2023;13:924-34.
13. Moon JI, Choi BH, Baek HJ, Ryu KH, Park SE, Ha JY, Jung EJ, Lee HS, An HJ. Comprehensive analyses with radiological and biological markers of breast cancer on contrast-enhanced chest CT: a single center experience using dual-layer spectral detector CT. Eur Radiol 2020;30:2782-90.
14. Barbara Krug K, Schömig-Markiefka B, Campbell GM, Püsken M, Maintz D, Schlamann M, Klein K, Gabriel Schafigh D, Malter W, Hellmich M. Correlation of CT-data derived from multiparametric dual-layer CT-maps with immunohistochemical biomarkers in invasive breast carcinomas. Eur J Radiol 2022;156:110544.
15. Zhang X, Zheng C, Yang Z, Cheng Z, Deng H, Chen M, Duan X, Mao J, Shen J. Axillary Sentinel Lymph Nodes in Breast Cancer: Quantitative Evaluation at Dual-Energy

CT. Radiology 2018;289:337-46.
16. Hammond ME, Hayes DF, Dowsett M, Allred DC, Hagerty KL, Badve S, *et al.* American Society of Clinical Oncology/College of American Pathologists guideline recommendations for immunohistochemical testing of estrogen and progesterone receptors in breast cancer. Arch Pathol Lab Med 2010;134:907-22.
17. Goldhirsch A, Winer EP, Coates AS, Gelber RD, Piccart-Gebhart M, Thürlimann B, Senn HJ; Panel members. Personalizing the treatment of women with early breast cancer: highlights of the St Gallen International Expert Consensus on the Primary Therapy of Early Breast Cancer 2013. Ann Oncol 2013;24:2206-23.
18. Goldhirsch A, Wood WC, Coates AS, Gelber RD, Thürlimann B, Senn HJ; Panel members. Strategies for subtypes--dealing with the diversity of breast cancer: highlights of the St. Gallen International Expert Consensus on the Primary Therapy of Early Breast Cancer 2011. Ann Oncol 2011;22:1736-47.
19. Dowsett M, Nielsen TO, A'Hern R, Bartlett J, Coombes RC, Cuzick J, *et al.* Assessment of Ki67 in breast cancer: recommendations from the International Ki67 in Breast Cancer working group. J Natl Cancer Inst 2011;103:1656-64.
20. Ogino I, Tayama Y, Arai M, Inoue T, Shimizu D, Ishikawa T. CT assessment of breast cancer for pathological involvement of four or more axillary nodes. Breast Cancer 2012;19:125-30.
21. Lowes S, Leaver A, Cox K, Satchithananda K, Cosgrove D, Lim A. Evolving imaging techniques for staging axillary lymph nodes in breast cancer. Clin Radiol 2018;73:396-409.
22. Cen D, Xu L, Li N, Chen Z, Wang L, Zhou S, Xu B, Liu CL, Liu Z, Luo T. BI-RADS 3-5 microcalcifications can preoperatively predict breast cancer HER2 and Luminal a molecular subtype. Oncotarget 2017;8:13855-62.
23. Horvat JV, Bernard-Davila B, Helbich TH, Zhang M, Morris EA, Thakur SB, Ochoa-Albiztegui RE, Leithner D, Marino MA, Baltzer PA, Clauser P, Kapetas P, Bago-Horvath Z, Pinker K. Diffusion-weighted imaging (DWI) with apparent diffusion coefficient (ADC) mapping as a quantitative imaging biomarker for prediction of immunohistochemical receptor status, proliferation rate, and molecular subtypes of breast cancer. J Magn Reson Imaging 2019;50:836-46.
24. An YY, Kim SH, Kang BJ, Park CS, Jung NY, Kim JY. Breast cancer in very young women (<30 years): Correlation of imaging features with clinicopathological features and immunohistochemical subtypes. Eur J Radiol 2015;84:1894-1902.
25. Uslu H, Önal T, Tosun M, Arslan AS, Ciftci E, Utkan NZ. Intravoxel incoherent motion magnetic resonance imaging for breast cancer: A comparison with molecular subtypes and histological grades. Magn Reson Imaging 2021;78:35-41.
26. Miyake KK, Nakamoto Y, Kanao S, Tanaka S, Sugie T, Mikami Y, Toi M, Togashi K. Journal Club: Diagnostic value of (18)F-FDG PET/CT and MRI in predicting the clinicopathologic subtypes of invasive breast cancer. AJR Am J Roentgenol 2014;203:272-9.
27. Wu J, Zhang X, Jia Z, Zhou X, Qi R, Ji H, Sun J, Sun C, Teng Z, Lu G, Chen X. Combined 18F-FDG and 18F-Alfatide II PET May Predict Luminal B (HER2 Negative) Subtype and Nonluminal Subtype of Invasive Breast Cancer. Mol Pharm 2022;19:3405-11.
28. Deniffel D, Sauter A, Dangelmaier J, Fingerle A, Rummeny EJ, Pfeiffer D. Differentiating intrapulmonary metastases from different primary tumors via quantitative dual-energy CT based iodine concentration and conventional CT attenuation. Eur J Radiol 2019;111:6-13.
29. Wang X, Liu D, Zeng X, Jiang S, Li L, Yu T, Zhang J. Dual-energy CT quantitative parameters for the differentiation of benign from malignant lesions and the prediction of histopathological and molecular subtypes in breast cancer. Quant Imaging Med Surg 2021;11:1946-57.
30. Wang X, Liu D, Zeng X, Jiang S, Li L, Yu T, Zhang J. Dual-energy CT quantitative parameters for evaluating Immunohistochemical biomarkers of invasive breast cancer. Cancer Imaging 2021;21:4.
31. Li Y, Yang ZG, Chen TW, Chen HJ, Sun JY, Lu YR. Peripheral lung carcinoma: correlation of angiogenesis and first-pass perfusion parameters of 64-detector row CT. Lung Cancer 2008;61:44-53.
32. van Hamersvelt RW, Eijsvoogel NG, Mihl C, de Jong PA, Schilham AMR, Buls N, Das M, Leiner T, Willemink MJ. Contrast agent concentration optimization in CTA using low tube voltage and dual-energy CT in multiple vendors: a phantom study. Int J Cardiovasc Imaging 2018;34:1265-75.
33. Acheampong T, Kehm RD, Terry MB, Argov EL, Tehranifar P. Incidence Trends of Breast Cancer Molecular Subtypes by Age and Race/Ethnicity in the US From 2010 to 2016. JAMA Netw Open 2020;3:e2013226.
34. Wang F, Wang D, Xu Y, Jiang H, Liu Y, Zhang J. Potential of the Non-Contrast-Enhanced Chest CT Radiomics

to Distinguish Molecular Subtypes of Breast Cancer: A Retrospective Study. Front Oncol 2022;12:848726.
35. Wu J, Ge L, Jin Y, Wang Y, Hu L, Xu D, Wang Z. Development and validation of an ultrasound-based radiomics nomogram for predicting the luminal from non-luminal type in patients with breast carcinoma. Front Oncol 2022;12:993466.

Cite this article as: Liu J, Wang L, Ai Z, Jian L, Yang M, Liu S, Yu X. A prediction model based on dual-layer spectral detector computed tomography for distinguishing nonluminal from luminal invasive breast cancer. Quant Imaging Med Surg 2024;14(12):8672-8685. doi: 10.21037/qims-24-598